Dynamical charge susceptibility of the spinless Falicov-Kimball model

J. K. Freericks and P. Miller
Department of Physics, Georgetown University, Washington, D.C. 20057-0995
(Received 4 May 2000)

An exact solution is presented for the frequency-dependent charge susceptibility of the spinless Falicov-Kimball model by using dynamical mean-field theory. We develop a nontrivial application of the Baym-Kadanoff ''conserving approximation'' formalism to exactly determine the frequency-dependent vertex function (which turns out to assume a particularly simple form). We show how the static and dynamic susceptibilities are decoupled in this model and how the dynamic susceptibility generically does not show any signal of the low-temperature charge-density-wave phase transition. We also examine the temperature evolution of the dynamic charge susceptibility for the special case of half-filling.

I. INTRODUCTION

The Falicov-Kimball model[1] was introduced in 1969 as a thermodynamic model for metal-insulator transitions in systems that have two different types of electrons—itinerant conduction electrons and localized *f* electrons. Twenty years later, Brandt and Mielsch[2] solved the Falicov-Kimball model exactly in the limit of infinite dimensions by using dynamical mean-field theory and the Baym-Kadanoff formalism. They also showed how to calculate static susceptibilities and found an Ising-like phase transition to a chessboard charge-density-wave phase at half-filling. Freericks[3] then showed that the system also displayed incommensurate order and phase separation at other fillings.

The Hamiltonian of the spinless Falicov-Kimball model[1] is

$$\hat{H}=-\frac{t^*}{2\sqrt{d}}\sum_{\langle i,j\rangle} d_i^\dagger d_j+\epsilon_f\sum_i w_i-\mu\sum_i (d_i^\dagger d_i+w_i)$$
$$+U\sum_i d_i^\dagger d_i w_i, \tag{1}$$

where $d_i^\dagger$ (d_i) is the spinless conduction electron creation (annihilation) operator at lattice site i and $w_i=0$ or 1 is a classical variable corresponding to the localized *f*-electron number at site *i*. The hopping matrix between nearest neighbors $\langle i,j\rangle$ (on a hypercubic lattice in d dimensions,[4] with $d\to\infty$) is $-t^*/(2\sqrt{d})$ with t^* chosen as our energy unit, ϵ_f is the localized electron level, μ is the chemical potential, and U is the mutual electron repulsion when a conduction electron and a localized *f*-electron both occupy the same lattice site.

In this contribution we examine the *d*-electron dynamical charge susceptibility [where $n_i(\tau)=\exp(\tau\hat{H})n_i(0)\exp(-\tau\hat{H})$ and $n_i=d_i^\dagger d_i$]

$$\chi(\mathbf{q},i\nu_l)=\mathrm{Tr}\,T_\tau\sum_{j,k}\int_0^\beta d\tau\, e^{i\nu_l\tau}e^{i\mathbf{q}\cdot(\mathbf{R}_j-\mathbf{R}_k)}$$
$$\times\left[\frac{\langle e^{-\beta\hat{H}}n_j(\tau)n_k(0)\rangle}{Z}-\frac{\langle e^{-\beta\hat{H}}n_j\rangle}{Z}\frac{\langle e^{-\beta\hat{H}}n_k\rangle}{Z}\right] \tag{2}$$

and its analytic continuation to the real-frequency axis. Here $i\nu_l=2i\pi Tl$ is the Bosonic Matsubara frequency, Z is the partition function, and $\mathbf{R}_j$ is the position operator for lattice site *j*. The Falicov-Kimball model is the simplest many-body problem that has nontrivial dynamics. The model is simple enough that an exact solution can be found for the charge susceptibility, but is complicated enough to show many-body effects. Shvaika[5] has shown how to determine the lattice charge susceptibility from a diagrammatic analysis of the atomic problem. Here we provide an alternative derivation, stressing the Baym-Kadanoff approach (which produces a much simpler form for the vertex), and we provide numerical results to complement the formalism.

We begin with a discussion of some special symmetries of the Falicov-Kimball model. Since the total conduction electron number is a conserved quantity, we find that $\Sigma_j n_j(\tau)=\Sigma_j n_j(0)$ has no τ dependence. Hence, the uniform charge susceptibility ($\mathbf{q}=\mathbf{0}$) vanishes for all nonzero frequencies. Similarly, the local *f* occupation is also conserved $[w_i(\tau)=w_i(0)]$, since w_i commutes with the lattice Hamiltonian. This implies that both the *ff* charge susceptibility and the mixed *df* charge susceptibility have no τ dependence and therefore are static, with no frequency dependence. Furthermore, a simple application of the chain rule and the definition of each of the susceptibilities as a derivative of the corresponding average electron filling with respect to an external field, shows that there is a discontinuity in the *dd* charge susceptibility at zero frequency[5] due to the coupling of the *d* and *f* electrons. This implies that there is a decoupling between the static and dynamic *dd* charge susceptibility.

The solution of the Falicov-Kimball model has been outlined in detail elsewhere.[2,3,6] Here we summarize the main points to establish our notation. The local Green's function at the fermionic Matsubara frequency $i\omega_n=i\pi T(2n+1)$ is defined by

$$G_n=G(i\omega_n)$$
$$=-\mathrm{Tr}_d\,\mathrm{Tr}_f\,T_\tau\int_0^\beta d\tau\, e^{i\omega_n\tau}\frac{\langle e^{-\beta\hat{H}_{at}}d(\tau)d^\dagger(0)S(\lambda)\rangle}{Z}, \tag{3}$$

with

$$Z = Z_0(\mu) + e^{-\beta(\epsilon_f-\mu)} Z_0(\mu - U), \tag{4}$$

the atomic partition function expressed in terms of

$$Z_0(\mu) = \mathrm{Tr}_d \langle e^{-\beta \hat{H}_0} S(\lambda) \rangle, \quad \hat{H}_0 = -\mu d^\dagger d. \tag{5}$$

In the above equations, the atomic Hamiltonian $\hat{H}_{at}$ is the Hamiltonian of Eq. (1) restricted to one site, with $t^*=0$, and all time dependence is with respect to this atomic Hamiltonian. The evolution operator $S(\lambda)$ satisfies

$$S(\lambda) = \exp\left[-\int_0^\beta d\tau \int_0^\beta d\tau' d^\dagger(\tau) \lambda(\tau - \tau') d(\tau') \right], \tag{6}$$

with $\lambda(\tau-\tau')$ a time-dependent atomic field adjusted to make the atomic Green's function equal to the local lattice Green's function. We define an effective medium by

$$G_0^{-1}(i\omega_n) = G_n^{-1} + \Sigma_n = i\omega_n + \mu - \lambda_n, \tag{7}$$

with Σ_n the local self-energy and λ_n the Fourier transform of $\lambda(\tau)$. The trace in Eq. (3) can be evaluated directly to yield

$$G_n = w_0 G_0(i\omega_n) + w_1 [G_0^{-1}(i\omega_n) - U]^{-1}, \tag{8}$$

with $w_0 = 1 - w_1$ and

$$w_1 = \exp[-\beta(\epsilon_f - \mu)] Z_0(\mu - U)/Z. \tag{9}$$

The self-consistency relation needed to determine λ_n and hence G_n is to equate the local lattice Green's function to the atomic Green's function via

$$G_n = \int_{-\infty}^{\infty} d\epsilon \frac{\rho(\epsilon)}{i\omega_n + \mu - \Sigma_n - \epsilon}, \tag{10}$$

with $\rho(\epsilon) = \exp(-\epsilon^2)/\sqrt{\pi}$ the noninteracting density of states for the infinite-dimensional hypercubic lattice.

The iterative algorithm to solve for G_n starts with $\Sigma_n = 0$. Then Eq. (10) is used to find G_n, Eq. (7) is employed to extract the effective medium, Eq. (8) is used to find a new local Green's function, and then Eq. (7) is used to find the new self-energy. The algorithm is then repeated until it converges, which usually requires only about a dozen or so iterations. In this contribution, we examine the half-filled case $\rho_d = \Sigma_i \langle n_i \rangle / N = 0.5$ and $\rho_f = \Sigma_i \langle w_i \rangle / N = 0.5$, which corresponds to $\mu = U/2$ and $\epsilon_f = -U/2$.

In the following section we illustrate how the Baym-Kadanoff formalism can be used to determine the dynamical charge susceptibility. Numerical results at half filling are presented in Sec. III and conclusions in Sec. IV.

II. BAYM-KADANOFF FORMALISM

The momentum-dependent susceptibility satisfies the following Dyson's equation:

$$\chi^{dd}(\mathbf{q}, i\omega_m, i\omega_n; i\nu_l) = \chi_0^{dd}(\mathbf{q}, i\omega_m; i\nu_l)\delta_{mn} - T\sum_{n'} \chi_0^{dd}(\mathbf{q}, i\omega_m; i\nu_l) \times \Gamma(i\omega_m, i\omega_{n'}; i\nu_l) \chi^{dd}(\mathbf{q}, i\omega_{n'}, i\omega_n; i\nu_l), \tag{11}$$

and the full susceptibility is found by summing over the fermionic Matsubara frequencies $\chi^{dd}(\mathbf{q}, i\nu_l) = T\Sigma_{mn} \chi^{dd}(\mathbf{q}, i\omega_m, i\omega_n; i\nu_l)$. In Eq. (11) the bare susceptibility satisfies

$$\chi_0^{dd}(X, i\omega_m; i\nu_l) = -\sum_{\mathbf{k}} G_m(\mathbf{k}) G_{m+l}(\mathbf{k}+\mathbf{q}) = -\frac{1}{\sqrt{1-X^2}} \int_{-\infty}^{\infty} d\epsilon \frac{\rho(\epsilon)}{i\omega_m + \mu - \Sigma_m - \epsilon} \times F_\infty\left(\frac{i\omega_{m+l} + \mu - \Sigma_{m+l} - X\epsilon}{\sqrt{1-X^2}} \right), \tag{12}$$

with $X(\mathbf{q}) = \lim_{d\to\infty} \Sigma_{i=1}^d \cos \mathbf{q}_i / d$ describing all of the momentum dependence of the susceptibility[7,2] and

$$F_\infty(z) = \int_{-\infty}^{\infty} d\epsilon \frac{\rho(\epsilon)}{z - \epsilon}, \tag{13}$$

the Hilbert transform of the noninteracting density of states.

The dynamical susceptibility simplifies in three cases: the chessboard case [$\mathbf{q} = (\pi, \pi, \ldots, \pi)$, $X = -1$] where

$$\chi_0^{dd}(-1, i\omega_m; i\nu_l) = -\frac{G_m + G_{m+l}}{i\omega_m + i\omega_{m+l} + 2\mu - \Sigma_m - \Sigma_{m+l}}; \tag{14}$$

the local case ($X = 0$) where

$$\chi_0^{dd}(0, i\omega_m; i\nu_l) = -G_m G_{m+l}; \tag{15}$$

and the uniform case [$\mathbf{q} = (0,0,\ldots,0)$, $X = 1$] where

$$\chi_0^{dd}(1, i\omega_m; i\nu_l) = -\frac{G_m - G_{m+l}}{i\nu_l + \Sigma_m - \Sigma_{m+l}}. \tag{16}$$

We will only be interested in these three simpler cases here. Note that in instances where the denominators of Eqs. (14) and (16) vanish, the susceptibility is evaluated by l'Hôpital's rule.

The calculation of the full susceptibility requires the local irreducible vertex function. The Baym-Kadanoff approach[8,9] solves for the irreducible vertex function in a manner that guarantees that an approximation scheme maintains the conservation laws of the Hamiltonian. The procedure requires that an approximate self-energy, $\Sigma(\mathbf{r}_1, \tau_1, \mathbf{r}_2, \tau_2)$ be given by the functional derivative of a free-energy functional, Φ, with respect to the full Green's function, $G(\mathbf{r}_1, \tau_1, \mathbf{r}_2, \tau_2)$. That is,

$$\Sigma(\mathbf{r}_1, \tau_1, \mathbf{r}_2, \tau_2) = \frac{\delta \Phi}{\delta G(\mathbf{r}_1, \tau_1, \mathbf{r}_2, \tau_2)}, \tag{17}$$

and then differentiation of the self-energy with respect to the Green's function produces the irreducible vertex function

$$\Gamma(\mathbf{r}_1, \tau_1, \mathbf{r}_2, \tau_2; \mathbf{r}_3, \tau_3, \mathbf{r}_4, \tau_4) = \frac{\delta \Sigma(\mathbf{r}_1, \tau_1, \mathbf{r}_2, \tau_2)}{\delta G(\mathbf{r}_3, \tau_3, \mathbf{r}_4, \tau_4)}. \tag{18}$$

Of course, this technique can also be used for an exact solution as we do here.

The dynamical-mean-field approximation for the Falicov-Kimball model in a spatially invariant system yields an exact expression for the self-energy $\Sigma = G_0^{-1} - G^{-1}$ [as seen in Eq. (7)] and we do not need to find the appropriate free-energy functional Φ. Our strategy is to calculate the Green's function of the effective medium, $G_0(\tau_1,\tau_2)$, when there is an additional time-dependent field, $\chi(\tau)$, which couples to the charge density, $d(\tau)d^\dagger(\tau)$ [i.e., we add $\int_0^\beta d\tau\,\chi(\tau)d^\dagger(\tau)d(\tau)$ to the exponent of the evolution operator in Eq. (6)]. This time-dependent field removes time-translational invariance from the system, so the Green's functions now depend on τ_1 and τ_2 separately. Using $G_0(\tau_1,\tau_2)$, we evaluate the self-energy as an explicit function of the full Green's function, $G(\tau_1,\tau_2)$, including terms to linear order in $\chi(\tau)$. We take the derivative of the self-energy with respect to the full Green's function to obtain the vertex function and afterwards set the field, $\chi(\tau)$ to zero. The calculation differs from standard approaches, in that $\chi(\tau)$ provides a time-dependence so that $G_0(\tau_1,\tau_2)$ depends separately on τ_1 and τ_2, not just on the difference, $(\tau_1 - \tau_2)$.

To begin, we introduce an auxiliary Green's function[10] (as Brandt and Urbanek did in their calculation of the f spectral function) in the presence of just the charge-coupled field, χ, defined by

$$g_{aux}(\tau_1,\tau_2;\mu) = \frac{-\mathrm{Tr}_d\, T_\tau\left\langle e^{-\beta\hat{H}_0}\exp\left(\int_0^\beta d\bar{\tau}\,\chi(\bar{\tau})d^\dagger(\bar{\tau})d(\bar{\tau})\right)d(\tau_1)d^\dagger(\tau_2)\right\rangle}{1+e^{\beta\mu}\exp\left(\int_0^\beta d\bar{\tau}\,\chi(\bar{\tau})\right)}, \tag{19}$$

where $\hat{H}_0 = -\mu d^\dagger d$, and we expand the time-dependent field, χ, in a Fourier series of the Bosonic frequencies

$$\chi(\tau) = \sum_l \chi_l e^{i\nu_l\tau}. \tag{20}$$

Noting that $d(\tau) = e^{\tau\hat{H}_0}d(0)e^{-\tau\hat{H}_0} = e^{\tau\mu}d(0)$, and taking into account the time ordering, we can easily perform the trace in Eq. (19), which yields (to linear order in χ_l):

$$g_{aux}(\tau_1,\tau_2;\mu) = e^{\mu(\tau_1-\tau_2)}\left[1+\sum_{l\neq 0}\frac{\chi_l}{i\nu_l}(e^{i\nu_l\tau_1}-e^{i\nu_l\tau_2})\right] \times\left[\frac{-\theta(\tau_1-\tau_2)}{1+e^{\beta\mu}e^{\beta\chi_0}}+\frac{\theta(\tau_2-\tau_1)}{1+e^{-\beta\mu}e^{-\beta\chi_0}}\right], \tag{21}$$

which depends on both τ_1 and τ_2 (not just $\tau_1-\tau_2$) because of the terms with $\chi_{l\neq 0}$. Nevertheless, the following symmetries are readily proven: for $\tau_1 < \tau_2 < \tau_1 + \beta$,

$$g_{aux}(\tau_1+\beta,\tau_2;\mu) = -g_{aux}(\tau_1,\tau_2;\mu), \tag{22}$$

and for $\tau_2 < \tau_1 < \tau_2 + \beta$,

$$g_{aux}(\tau_1,\tau_2+\beta;\mu) = -g_{aux}(\tau_1,\tau_2;\mu). \tag{23}$$

Hence we can find the Fourier transform of $g_{aux}(\tau_1,\tau_2;\mu)$ in terms of the fermionic Matsubara frequencies

$$g_{aux}(i\omega_n, i\omega_{n'};\mu) = T\int_0^\beta d\tau_1\int_{-\beta+\tau_1}^{\tau_1} d\tau_2 e^{i\omega_n\tau_1}e^{-i\omega_{n'}\tau_2}g_{aux}(\tau_1,\tau_2;\mu). \tag{24}$$

The result is that $g_{aux}(i\omega_n, i\omega_{n'};\mu)$ contains terms that are diagonal in n,n' and terms shifted off the diagonal by l that are proportional to χ_l:

$$g_{aux}(i\omega_n, i\omega_{n'};\mu) = \frac{\delta_{n,n'}}{i\omega_n+\mu} + \sum_l \frac{\delta_{n+l,n'}\chi_l}{i\nu_l} \times\left(\frac{1}{i\omega_{n'}+\mu}-\frac{1}{i\omega_n+\mu}\right). \tag{25}$$

The Green's function for the effective medium of the atomic problem, $G_0(\tau_1,\tau_2)$, is obtained as before by including a local time-dependent field, $\lambda(\tau-\tau')$, which incorporates the effects of propagation on the lattice and only depends on the time difference:

$$G_0(\tau_1,\tau_2) = \frac{-\mathrm{Tr}_d T_\tau\left\langle e^{-\beta\hat{H}_0}\exp\left(\int_0^\beta d\bar{\tau}\,\chi(\bar{\tau})d^\dagger(\bar{\tau})d(\bar{\tau})\right)S(\lambda)d(\tau_1)d^\dagger(\tau_2)\right\rangle}{Z_0(\mu)}, \tag{26}$$

where we restrict $\chi(\tau)$ such that $\chi_0=0$. As the local field only contains diagonal frequency components, $\lambda(i\omega_n)\delta_{nn'}$, the effective-medium Green's function is easily obtained from the auxiliary Green's function through:

$$[G_0]^{-1}_{n,n'}=[g_{aux}(\mu)]^{-1}_{n,n'}-\lambda(i\omega_n)\delta_{n,n'}, \tag{27}$$

where the Green's function matrices are inverted in frequency coordinates, such that $[G_0]^{-1}_{n,n'}$ represents the n,n' components of the inverse of the matrix $G_0(i\omega_n,i\omega_{n'})$. A key aspect of our derivation of the vertex function is that to linear order in a single-frequency component of the charge-coupled field, χ_l, the Green's function for the effective medium, $G_0(i\omega_n,i\omega_{n'})$, like the auxiliary Green's function, $g_{aux}(i\omega_n,i\omega_{n'};\mu)$, only contains components in the two diagonals given by $\delta_{n,n'}$ and $\delta_{n+l,n'}$.

The full Green's function is defined by

$$G(\tau_1,\tau_2)=\frac{-\mathrm{Tr}_f\,\mathrm{Tr}_d\,T_\tau\left\langle e^{-\beta\hat{H}_{at}}\exp\left(\int_0^\beta d\bar{\tau}\,\chi(\bar{\tau})d^\dagger(\bar{\tau})d(\bar{\tau})\right)S(\lambda)d(\tau_1)d^\dagger(\tau_2)\right\rangle}{Z}, \tag{28}$$

where Z is given by Eq. (4) and the time dependence of the d operators is governed by $\hat{H}_{at}$ (we assume $\chi_0=0$ again). The Green's function contains a trace over f-electron states, which leads to two terms:

$$G(\tau_1,\tau_2)=\frac{-\mathrm{Tr}_d\,T_\tau\left\langle e^{-\beta\hat{H}_0}\exp\left(\int_0^\beta d\bar{\tau}\,\chi(\bar{\tau})d^\dagger(\bar{\tau})d(\bar{\tau})\right)S(\lambda)d(\tau_1)d^\dagger(\tau_2)\right\rangle}{Z} \tag{29}$$

$$+e^{-\beta(\epsilon_f-\mu)}\frac{-\mathrm{Tr}_d\,T_\tau\left\langle e^{-\beta\hat{H}_1}\exp\left(\int_0^\beta d\bar{\tau}\,\chi(\bar{\tau})d^\dagger(\bar{\tau})d(\bar{\tau})\right)S(\lambda)d(\tau_1)d^\dagger(\tau_2)\right\rangle}{Z}, \tag{30}$$

where $\hat{H}_0=-\mu d^\dagger d$ is the atomic Hamiltonian with no f electrons, and $\hat{H}_1=(U-\mu)d^\dagger d$ is the atomic Hamiltonian for d electrons in the presence of one f electron.

We can now relate the full Green's function to the Green's function of the effective medium through the following matrix equation:

$$G(i\omega_n,i\omega_{n'})=w_0G_0(i\omega_n,i\omega_{n'})+w_1[(G_0^{-1})-U]^{-1}_{n,n'}, \tag{31}$$

where $w_0=1-w_1$ and w_1 are given by Eq. (9) and equal the fraction of sites with an occupancy of zero and one f electron, respectively. In the above, and all following equations, U is the only matrix that is necessarily diagonal in frequency space.

Equation (31) can be rearranged by multiplying on the left or right by matrices such as G^{-1}, G_0^{-1}, and $G_0^{-1}-U$ to give the two following matrix equations (with indices suppressed):

$$G_0^{-2}-(U+G^{-1})G_0^{-1}+(1-w_1)UG^{-1}=0, \tag{32}$$

$$G_0^{-2}-G_0^{-1}(U+G^{-1})+(1-w_1)UG^{-1}=0. \tag{33}$$

Adding these two equations together and collecting terms (noting the noncommutativity and hence the ordering of the matrices) then yield the following quadratic matrix equation:

$$\left[G_0^{-1}-\frac{1}{2}(U+G^{-1})\right]^2-\frac{1}{4}(U+G^{-1})^2+(1-w_1)UG^{-1}=0. \tag{34}$$

Substitution for G_0 by Σ, using Dyson's equation in the form

$$\Sigma(i\omega_n,i\omega_m)=[G_0^{-1}]_{n,m}-[G^{-1}]_{n,m}, \tag{35}$$

yields

$$\left[\Sigma+\frac{1}{2}(G^{-1}-U)\right]^2=\frac{1}{4}[U^2+2(2w_1-1)UG^{-1}+G^{-2}], \tag{36}$$

where each term in G and Σ is a matrix in frequency space and U multiplies the identity matrix. Note that in the limit $\chi_l=0$, Eq. (36) becomes diagonal and reduces to the conventional quadratic expression for the self-energy in terms of $G(i\omega_n)$ and w_1 as first determined by Brandt and Mielsch.[2]

The irreducible vertex function is defined in frequency space by

$$\Gamma(i\omega_n,i\omega_m;i\omega_{n'},i\omega_{m'})=T^4\int_0^\beta d\tau_1\int_{\tau_1}^{\beta+\tau_1}d\tau_2\int_0^\beta d\tau_{1'}\int_{\tau_{1'}}^{\beta+\tau_{1'}}d\tau_{2'}\times e^{i\omega_n\tau_1-i\omega_m\tau_2+i\omega_{n'}\tau_{1'}-i\omega_{m'}\tau_{2'}}\Gamma(\tau_1,\tau_2;\tau_{1'},\tau_{2'}). \tag{37}$$

As the vertex function is independent of the absolute time, we can change variables, $\tau_1 \mapsto \tau_1 - \tau_{2'}, \tau_2 \mapsto \tau_2 - \tau_{2'}, \tau_{1'} \mapsto \tau_{1'} - \tau_{2'}$, so that the $\tau_{2'}$ integral yields a δ function that requires $i\omega_{m'} = i\omega_n - i\omega_m + i\omega_{n'}$. Hence, given the difference between two fermionic Matsubara frequencies, $i\omega_m - i\omega_n = i\nu_l$, is a bosonic frequency, the vertex function becomes

$$\Gamma(i\omega_n, i\omega_{n'}; i\nu_l) = \frac{1}{T} \frac{\delta\Sigma(i\omega_n, i\omega_n + i\nu_l)}{\delta G(i\omega_{n'}, i\omega_{n'} + i\nu_l)}. \tag{38}$$

The problem is greatly simplified by calculating $\Sigma_{n,m}$ to first order in χ, for a single-frequency component, χ_l. In this case, both $\Sigma_{n,m}$ and $G_{n,m}$ contain diagonal terms, and off-diagonal terms linear in χ_l where $m = n + l$, so that

$$\begin{aligned} \Sigma_{n,m} &= \Sigma_n \delta_{n,m} + \overline{\Sigma}_n \delta_{n+l,m}, \\ G_{n,m} &= G_n \delta_{n,m} + \overline{G}_n \delta_{n+l,m}. \end{aligned} \tag{39}$$

We are interested in the case where $l \neq 0$, as the zero-frequency response (corresponding to a shift of the chemical potential) is well known.[2,3,6]

Next, we calculate the diagonal and off-diagonal pieces of the self-energy. Equation (36) simplifies from a full quadratic matrix equation to the following coupled equations:

$$\left(\Sigma_n - \frac{U}{2} + \frac{1}{2G_n}\right)^2 = \frac{1}{4G_n^2}\{1 + 2UG_n(2w_1 - 1) + U^2 G_n^2\}, \tag{40}$$

$$\begin{aligned} &\left(\overline{\Sigma}_n - \frac{\overline{G}_n}{2G_n G_{n+l}}\right)\left(\Sigma_n + \frac{1}{2G_n} + \Sigma_{n+l} + \frac{1}{2G_{n+l}} - U\right) \\ &\quad = \frac{\overline{G}_n}{4G_n G_{n+l}}\left[2(1 - 2w_1)U - \frac{(G_n + G_{n+l})}{G_n G_{n+l}}\right]. \end{aligned} \tag{41}$$

Equation (40) contains only diagonal terms with no dependence on the finite-frequency field χ_l; hence Σ_n is unchanged from its value when $\chi_l = 0$. We concentrate on rearranging Eq. (41) to obtain the frequency-dependent response. First, we multiply both sides of Eq. (41) by

$$\left(\Sigma_n - \frac{U}{2} + \frac{1}{2G_n}\right) - \left(\Sigma_{n+l} - \frac{U}{2} + \frac{1}{2G_{n+l}}\right) \tag{42}$$

and use Eq. (40) to replace the quadratic terms on the left, giving

$$\begin{aligned} &\left(\overline{\Sigma}_n - \frac{\overline{G}_n}{2G_n G_{n+l}}\right)\left[2U(2w_1 - 1) + \frac{1}{G_n} + \frac{1}{G_{n+l}}\right] \\ &\quad \times \left(\frac{1}{4G_n} - \frac{1}{4G_{n+l}}\right) \\ &\quad = \frac{\overline{G}_n}{4G_n G_{n+l}}\left[2(1 - 2w_1)U - \frac{(G_n + G_{n+l})}{G_n G_{n+l}}\right] \\ &\quad \times \left(\Sigma_n + \frac{1}{2G_n} - \Sigma_{n+l} - \frac{1}{2G_{n+l}}\right). \end{aligned} \tag{43}$$

The above form gives rise to considerable cancellation between the two sides, leading to the amazingly simple result:

$$\overline{\Sigma}_n = \overline{G}_n \frac{\Sigma_n - \Sigma_{n+l}}{G_n - G_{n+l}}. \tag{44}$$

So the only terms in $\Sigma_{n,m}$ that depend on a finite frequency component, $i\nu_l$, of the χ field are $\Sigma_{n,n+l} = \overline{\Sigma}_n$. The only terms that survive the limit, $\chi_l \mapsto 0$ after differentiation, to give the vertex function, are

$$\begin{aligned} \Gamma(i\omega_n, i\omega_n; i\nu_l) &= \frac{1}{T} \frac{\delta\overline{\Sigma}(i\omega_n, i\omega_{n+l})}{\delta G(i\omega_n, i\omega_{n+l})} \\ &= \frac{1}{T} \frac{\delta\overline{\Sigma}_n}{\delta\overline{G}_n} = \frac{1}{T} \frac{\Sigma_n - \Sigma_{n+l}}{G_n - G_{n+l}}. \end{aligned} \tag{45}$$

The above simple result found from this Baym-Kadanoff analysis is identical to that found by diagrammatic calculations[5] that give the more complicated form:

$$\Gamma(i\omega_n, i\omega_n; i\nu_l) = \frac{1}{T} \frac{w_0 w_1 U^2}{(1 + G_n\Sigma_n)[1 + G_n(\Sigma_n - U)](1 + G_{n+l}\Sigma_{n+l})[1 + G_{n+l}(\Sigma_{n+l} - U)] + w_0 w_1 U^2 G_n G_{n+l}}. \tag{46}$$

The proof of this equivalence is presented in the Appendix.

Since the vertex function is diagonal, we have a simple form for the dynamical charge susceptibility

$$\chi^{dd}(X; i\nu_l \neq 0) = T\sum_m \frac{\chi_0(X, i\omega_m; i\nu_l)}{1 + \chi_0(X, i\omega_m; i\nu_l)\dfrac{\Sigma_m - \Sigma_{m+l}}{G_m - G_{m+l}}}. \tag{47}$$

In the limit $\mathbf{q} = \mathbf{0}$ $(X = 1)$, substitution of χ_0^{dd} from Eq. (16) into Eq. (47) gives

$$\chi^{dd}(1; i\nu_l \neq 0) = -T\sum_m \frac{G_m - G_{m+l}}{i\nu_l} = 0, \tag{48}$$

as expected by our symmetry arguments. Notice that χ_0^{dd} does not vanish; it is the vertex corrections that force the full susceptibility to vanish.

The final step in our formalism development is to perform the analytic continuation of Eq. (47) from the imaginary to the real axis. Our method is not completely rigorous, because we are unable to verify necessary analyticity arguments as described below, but we compare the direct calculation of the susceptibility on the imaginary axis to the inferred value there that is found by using the spectral formula from the real axis. In nearly all cases, we have accuracy to better than one part in 1000, which supports, *a posteriori*, that our technique is valid.

We will consider only the case with $X=-1$ here, since the $X=1$ susceptibility is trivial and since the $X=0$ case is simpler and can easily be worked out by following the same steps we use for the chessboard case. We start by replacing the summation over Matsubara frequencies in Eq. (47) by three contour integrals, which are chosen as in Fig. 1 to encircle all of the simple poles at the fermionic Matsubara frequencies and no other poles in the corresponding integrals [in other words, the only poles contributing are the simple poles from $f(\omega)$ below]. The susceptibility then becomes (for simplicity, we consider $\nu_l>0$ here)

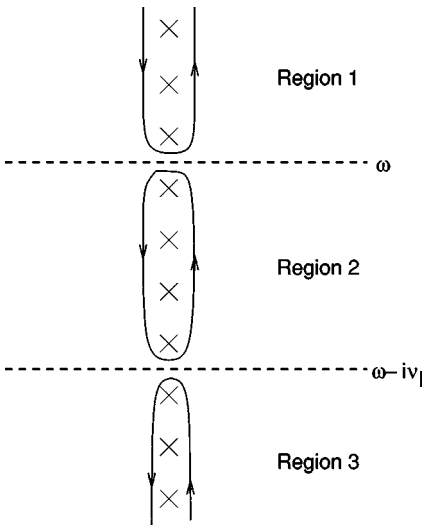

FIG. 1. Contour integral for evaluating the Matsubara frequency summations of the charge susceptibility. The ×'s mark the locations of fermionic Matsubara frequencies. The contours enclose all Matsubara frequencies, but no other poles of the system. Note that we divide the complex plane into three regions: (i) region 1, where the imaginary part is greater than zero; (ii) region 2, where the imaginary part lies between zero and $-i\nu_l$; and (iii) region 3, where the imaginary part is less than $-i\nu_l$.

$$\chi^{dd}(-1;i\nu_l)=\frac{i}{2\pi}\int_{C_1}d\omega\, f(\omega)\frac{\dfrac{G_R(\omega)+G_R(\omega+i\nu_l)}{2\omega+2\mu+i\nu_l-\Sigma_R(\omega)-\Sigma_R(\omega+i\nu_l)}}{1-\dfrac{G_R(\omega)+G_R(\omega+i\nu_l)}{2\omega+2\mu+i\nu_l-\Sigma_R(\omega)-\Sigma_R(\omega+i\nu_l)}\dfrac{\Sigma_R(\omega)-\Sigma_R(\omega+i\nu_l)}{G_R(\omega)-G_R(\omega+i\nu_l)}}$$

$$+\frac{i}{2\pi}\int_{C_2}d\omega\, f(\omega)\frac{\dfrac{G_A(\omega)+G_R(\omega+i\nu_l)}{2\omega+2\mu+i\nu_l-\Sigma_A(\omega)-\Sigma_R(\omega+i\nu_l)}}{1-\dfrac{G_A(\omega)+G_R(\omega+i\nu_l)}{2\omega+2\mu+i\nu_l-\Sigma_A(\omega)-\Sigma_R(\omega+i\nu_l)}\dfrac{\Sigma_A(\omega)-\Sigma_R(\omega+i\nu_l)}{G_A(\omega)-G_R(\omega+i\nu_l)}}$$

$$+\frac{i}{2\pi}\int_{C_3}d\omega\, f(\omega)\frac{\dfrac{G_A(\omega)+G_A(\omega+i\nu_l)}{2\omega+2\mu+i\nu_l-\Sigma_A(\omega)-\Sigma_A(\omega+i\nu_l)}}{1-\dfrac{G_A(\omega)+G_A(\omega+i\nu_l)}{2\omega+2\mu+i\nu_l-\Sigma_A(\omega)-\Sigma_A(\omega+i\nu_l)}\dfrac{\Sigma_A(\omega)-\Sigma_A(\omega+i\nu_l)}{G_A(\omega)-G_A(\omega+i\nu_l)}},\tag{49}$$

where $f(\omega)=1/[1+\exp(\beta\omega)]$ is the Fermi function and the subscript R or A refers to the retarded or advanced Green's function (or self-energy). The choices of the subscripts are so that the Green's functions and self-energies are analytic within regions 1, 2, or 3. Hence the contours can be deformed until they run parallel to the real axis, as shown in Fig. 2. We are making an assumption that there are no other poles present within these regions, when we deform the contours. In fact, if we make an analytic continuation of just the bare susceptibility, then after continuing $i\nu_l$ to $\nu+i\delta$ we do find a pole that lies in region 2 just below the real axis (at $\omega=-\nu/2-i\delta$), but the residue of this pole vanishes when ν lies on the real axis. It is more difficult to make such an analysis for the full susceptibility, so we rely instead on the comparison with the direct calculation on the imaginary axis.

When we evaluate the integrals along the lines indicated in Fig. 2, we will evaluate the Fermi function at $\omega-i\nu_l$, which we set equal to $f(\omega)$ before continuing the ν frequency. Then we can evaluate the final result, which becomes

$$\chi^{dd}(-1;\nu)=\frac{i}{2\pi}\int_{-\infty}^{\infty}d\omega\Bigg\{f(\omega)\frac{\dfrac{G(\omega)+G(\omega+\nu)}{2\omega+2\mu+\nu-\Sigma(\omega)-\Sigma(\omega+\nu)}}{1-\dfrac{G(\omega)+G(\omega+\nu)}{2\omega+2\mu+\nu-\Sigma(\omega)-\Sigma(\omega+\nu)}\dfrac{\Sigma(\omega)-\Sigma(\omega+\nu)}{G(\omega)-G(\omega+\nu)}}$$

$$-f(\omega+\nu)\frac{\dfrac{G^*(\omega)+G^*(\omega+\nu)}{2\omega+2\mu+\nu-\Sigma^*(\omega)-\Sigma^*(\omega+\nu)}}{1-\dfrac{G^*(\omega)+G^*(\omega+\nu)}{2\omega+2\mu+\nu-\Sigma^*(\omega)-\Sigma^*(\omega+\nu)}\dfrac{\Sigma^*(\omega)-\Sigma^*(\omega+\nu)}{G^*(\omega)-G^*(\omega+\nu)}}$$

$$-[f(\omega)-f(\omega+\nu)]\frac{\dfrac{G^*(\omega)+G(\omega+\nu)}{2\omega+2\mu+\nu-\Sigma^*(\omega)-\Sigma(\omega+\nu)}}{1-\dfrac{G^*(\omega)+G(\omega+\nu)}{2\omega+2\mu+\nu-\Sigma^*(\omega)-\Sigma(\omega+\nu)}\dfrac{\Sigma^*(\omega)-\Sigma(\omega+\nu)}{G^*(\omega)-G(\omega+\nu)}}\Bigg\}, \tag{50}$$

and we replaced the advanced functions by the complex conjugate of the retarded Green's function (which is valid on the real axis).

III. NUMERICAL RESULTS

We performed a number of different numerical calculations of the charge response. To begin, we summarize the *d*-electron spectral functions in the weak-coupling ($U=0.25$) limit, the moderate-coupling limit ($U=1$) and the strong-coupling limit ($U=4$), which are illustrated in Fig. 3. Note that the interacting density of states is temperature independent for this model (as first shown by Van Dongen[11]). In the weak-coupling case ($U=0.25$) the density of states looks Gaussian, with only small modifications due to the interactions. At moderate coupling, ($U=1$), we find that a pseudogap appears in the density of states at the chemical potential. Note that this is a correlation-induced pseudogap and is not resulting from the charge-density-wave order of the ground state, since these results are for the high-temperature homogeneous phase. Finally, a true gap develops in strong coupling ($U=4$), which rapidly approaches U as U increases in magnitude. In Fig. 4 we show plots of the static chessboard susceptibility for the three different values of U and inset a plot of the transition temperature as a function of $U/(U+t^*)$. The chain-dotted lines are guides to the eye for T_c at the three values of U. The transition temperature has a classic form—increasing for weak U, reaching a maximum at moderate U, and then decreasing in the strong-coupling regime. Notice how the static susceptibility diverges as we approach T_c because we are in the thermodynamic limit. In Fig. 5 we show the dynamical chessboard susceptibility at five different temperatures ranging from well above T_c to just above T_c. Notice how there is a temperature dependence to the charge susceptibility, but how

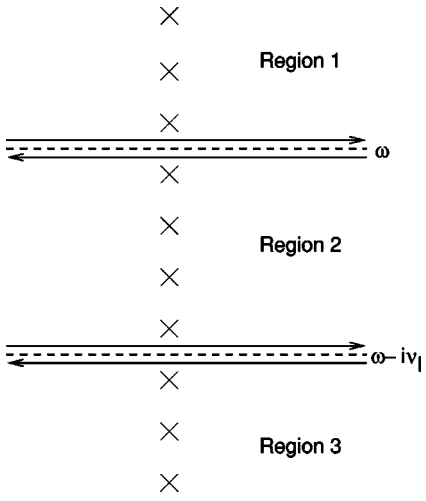

FIG. 2. Deformation of the contours needed for evaluation of the susceptibility on the real axis. The integrations are parallel to the real axis.

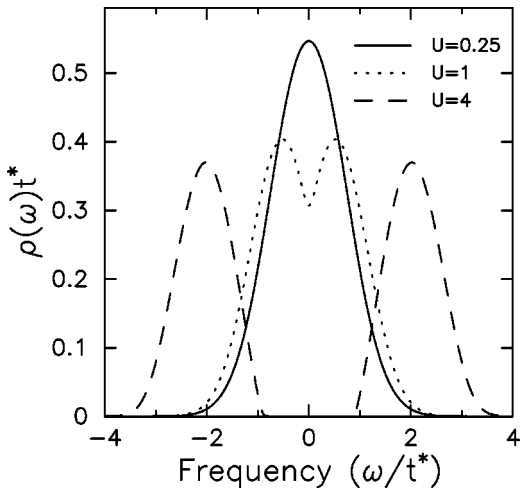

FIG. 3. Interacting density of states for the spinless Falicov-Kimball model at half filling and $U=0.25$ (solid line), $U=1$ (dotted line), $U=4$ (dashed line). Note how the density of states evolves from being essentially Gaussian to developing a pseudogap and then a real gap as the interaction strength is increased. The density of states is temperature independent for this model.

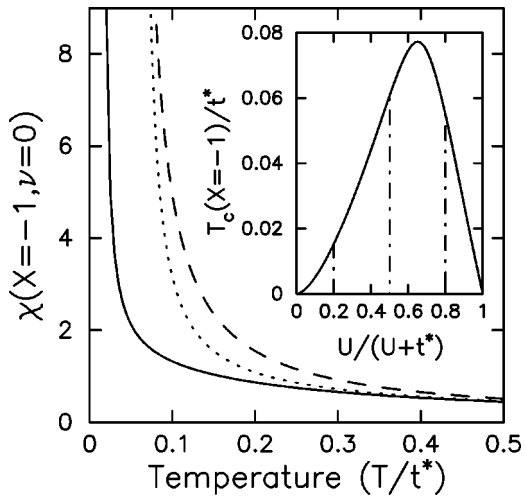

FIG. 4. Static charge susceptibility for the chessboard charge-density-wave plotted versus temperature for three values of U: (i) $U=0.25$, solid line, $T_c=0.0153$; (ii) $U=1$, dashed line, $T_c=0.0608$; and (iii) $U=4$, dotted line, $T_c=0.0547$. The inset is the charge-density-wave transition temperature plotted as a function of the interaction strength $U/(U+t^*)$.

there is no indication of the phase transition seen in the static susceptibility (recall the susceptibility is discontinuous at $\nu=0$ and we are only plotting the continuous piece of the susceptibility). In Fig. 6 we show the same plot for the local dynamical susceptibility. Its behavior is quite similar to that of the chessboard susceptibility, but with a less marked temperature dependence. The expected peak in the imaginary part at low frequencies due to quasiparticle excitations can be seen, and it has a classic ''triangular'' shape as expected

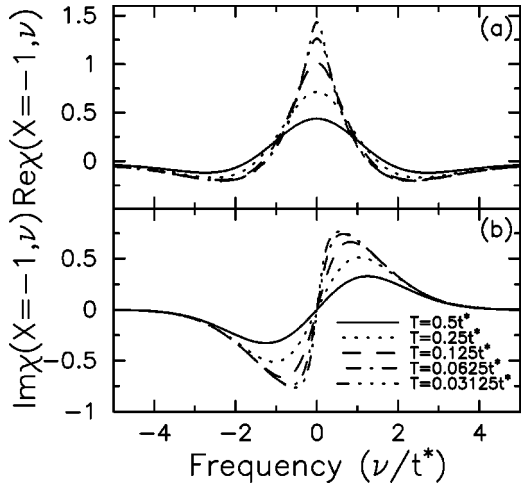

FIG. 5. Dynamical chessboard charge-density-wave susceptibility as a function of temperature for the case $U=0.25$. The real part is plotted in (a) and the imaginary part in (b). Five different temperatures are shown: $T=0.5$ (solid line), $T=0.25$ (dotted line), $T=0.125$ (dashed line), $T=0.0625$ (chain-dotted line), and $T=0.031\,25$ (chain-double-dotted line). The real part of the susceptibility becomes more sharply peaked at zero frequency, but shows no sign of diverging (because of the decoupling of the static and dynamic susceptibilities). The imaginary part sharpens as T is lowered, and has a shape reminiscent of that of a noninteracting system arising from the quasiparticle excitations.

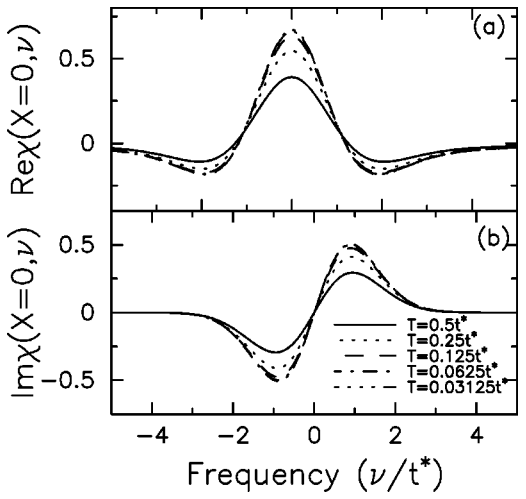

FIG. 6. Dynamical local charge-density-wave susceptibility as a function of temperature for the case $U=0.25$. The real part is plotted in (a) and the imaginary part in (b). Five different temperatures are shown: $T=0.5$ (solid line), $T=0.25$ (dotted line), $T=0.125$ (dashed line), $T=0.0625$ (chain-dotted line), and $T=0.031\,25$ (chain-double-dotted line). The form of the susceptibility is similar to the chessboard case, except the system reaches the low-temperature limit much more rapidly, and the imaginary part is pushed somewhat farther from zero frequency.

in a noninteracting system (recall the local susceptibility is the average over all momentum vectors, so we expect a linear contribution at small frequency and a curved drop off at high frequencies as we reach the approximate half bandwidth). The case of moderate coupling is shown in Figs. 7 and 8. Here, the chessboard susceptibility actually decreases as T is lowered because of the pseudogap in the density of states. Once again the temperature dependence of the local

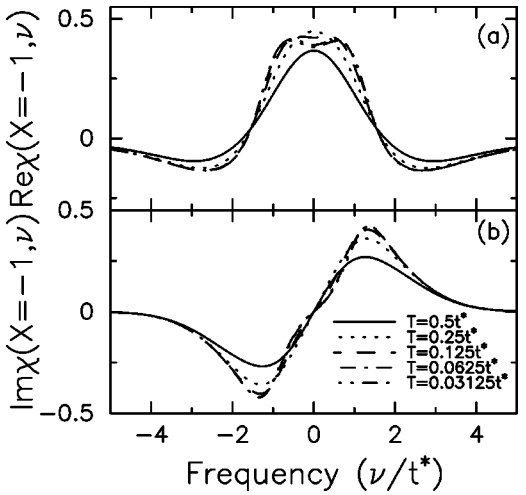

FIG. 7. Dynamical chessboard charge-density-wave susceptibility as a function of temperature for the case $U=1$. The real part is plotted in (a) and the imaginary part in (b). Five different temperatures are shown: $T=0.5$ (solid line), $T=0.25$ (dotted line), $T=0.125$ (dashed line), $T=0.0625$ (chain-dotted line), and $T=0.031\,25$ (chain-double-dotted line). The real part of the susceptibility initially increases as T is lowered at low frequencies, but then decreases and starts to develop additional peaks as the effects of the pseudogap are felt.

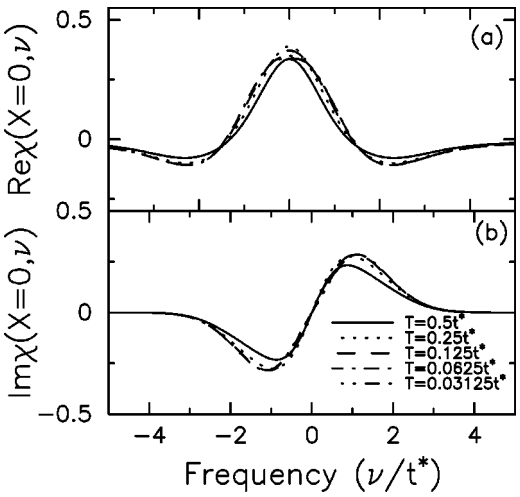

FIG. 8. Dynamical local charge-density-wave susceptibility as a function of temperature for the case $U=1$. The real part is plotted in (a) and the imaginary part in (b). Five different temperatures are shown: $T=0.5$ (solid line), $T=0.25$ (dotted line), $T=0.125$ (dashed line), $T=0.0625$ (chain-dotted line), and $T=0.031\,25$ (chain-double-dotted line). We once again see a similarity with the chessboard phase, but the temperature dependence is much reduced here.

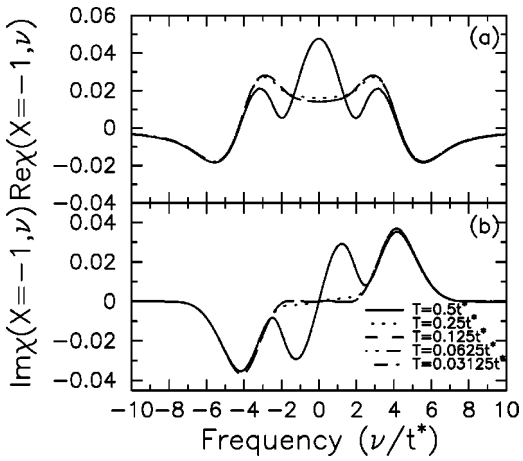

FIG. 9. Dynamical chessboard charge-density-wave susceptibility as a function of temperature for the case $U=4$. The real part is plotted in (a) and the imaginary part in (b). Five different temperatures are shown: $T=0.5$ (solid line), $T=0.25$ (dotted line), $T=0.125$ (dashed line), $T=0.0625$ (chain-dotted line), and $T=0.031\,25$ (chain-double-dotted line). Note how a substantial low-energy feature, present at $T=0.5$ disappears rapidly as T is lowered. The temperature scale for this evolution is on the order of $T\approx t^{*2}/U=0.25$. For temperatures below this energy scale the system's behavior is governed most strongly by the energy gap in the density of states. We find that the imaginary part of the charge susceptibility goes slightly negative over a frequency range around $0.5<\nu<2$, which we believe to be an artifact of the numerical analytic continuation procedure in the presence of a gap.

susceptibility is much less than the chessboard susceptibility (and we are including data below the T_c to the charge-density-wave instability). The development from a single low-energy peak in the real part to two nearly overlapping peaks (corresponding to charge transfer excitations) is clear even at moderate coupling where the density of states has only a pseudogap. Note once again that these peak developments arise from correlation effects and not from an underlying charge-density-wave order because these calculations are all performed within the homogeneous phase (even when we go below T_c).

In Figs. 9 and 10 we show the results at strong coupling $U=4$. The charge susceptibility shows a number of interesting new features in the strong-coupling regime. The charge-transfer peaks, which are easiest seen as broad peaks in the imaginary part of the susceptibility, are present at the expected locations of $\pm U$. At high temperatures, the system has a large peak in the real part of the susceptibility near zero frequency, which rapidly decreases as T is lowered, and becomes unnoticable at low temperatures. The imaginary part goes from having a linear behavior at low frequency to being essentially zero. Hence, in addition to the energy scale of the order of U (corresponding to the large charge-transfer peaks in the imaginary part of the susceptibility) there is a low-energy scale on the order of t^{*2}/U that determines the low-temperature evolution of the charge excitations and the energy scale of those low-energy excitations. The high-energy features are ''frozen in'' at a high temperature scale, and there is strong temperature evolution in the low-frequency regime until T becomes smaller than the low-energy scale where the low-energy features are ''frozen in.'' We believe these low-energy charge excitations are associated with virtual hopping processes, where an electron virtually hops onto a site occupied by a localized electron, and then hops off that site. Such processes turn off at temperatures below t^{*2}/U. Once again the dependence of the chessboard and the local susceptibilities are similar and there is no signal of the phase transition in the dynamical piece of the charge susceptibility. We find that we lose some accuracy in our calculations at strong coupling, perhaps arising from the gap in the density of states and its effect on the low-temperature charge dynamics. Another possibility is that there are additional poles and

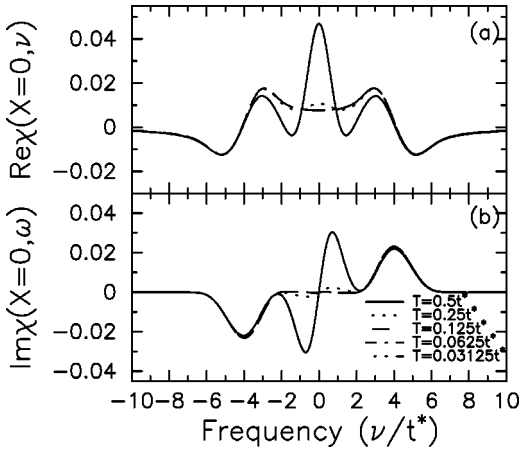

FIG. 10. Dynamical local charge-density-wave susceptibility as a function of temperature for the case $U=4$. The real part is plotted in (a) and the imaginary part in (b). Five different temperatures are shown: $T=0.5$ (solid line), $T=0.25$ (dotted line), $T=0.125$ (dashed line), $T=0.0625$ (chain-dotted line), and $T=0.031\,25$ (chain-double-dotted line). The results here are similar to those for the chessboard susceptibility, except here we have a slower temperature dependence, as a $\nu=0$ peak in the real part of the charge susceptibility can still be seen at $T=0.25$, and it has already vanished in the chessboard case.

residues that need to be taken into account in our ''approximate'' analytic continuation. One illustration of the numerical difficulties is that we no longer have an accuracy of one part in a thousand (it is typically a few parts in a thousand) when we evaluate the charge susceptibility on the imaginary axis by using the spectral formula and comparing with a direct calculation on the imaginary axis. Another illustration is that at the lowest temperatures the imaginary part of the spectral function becomes slightly negative for a frequency range in the vicinity of $0.5<\nu<2$ (where the imaginary part is approximately -0.0003), which must be an artifact of the approximate analytic continuation due to the fact that the spectral function is known to be nonnegative for positive values of the frequency.

IV. CONCLUSIONS

We have presented a nontrivial example of the Baym-Kadanoff formalism to derive the dynamical susceptibilities of the Falicov-Kimball model. The dynamical susceptibility breaks into two pieces, a static piece that reflects the coupling of the system to the charge-density-wave distortions, and a frequency-dependent piece, which is less affected by any underlying charge-density-wave order. We developed the formalism to evaluate this frequency-dependent piece of the susceptibility exactly on the imaginary axis. We also developed an analytic-continuation scheme that we were unable to establish with full rigor due to the possibility of a small contribution from neglected residues of poles that could arise within the analytic-continuation procedure, but which is nevertheless quite accurate over a wide range of parameters.

We find a number of interesting properties of this model: (1) the static and dynamical susceptibilities are decoupled—the static susceptibility diverges at T_c, but no signal of this phase transition is seen in the dynamical susceptibility; (2) the momentum dependence of the dynamical susceptibility is not too strong around the chessboard point—we see little variation between the $X=-1$ and $X=0$ susceptibilities, but the $X=1$ susceptibility vanishes by symmetry, so momentum dependence is stronger near the Brillouin zone center; and (3) the dynamical susceptibilities do possess temperature dependence even though the interacting density of states is temperature independent. The temperature dependence is most striking in the strong-coupling regime where a low-energy scale on the order of t^{*2}/U arises and the charge susceptibility has a strong temperature dependence near this approximate temperature.

Our application of the Baym-Kadanoff formalism provides an interesting counterpoint to the diagrammatic derivation about the atomic limit, and can be applied to other related problems where the so-called ''static approximation'' is exact. We have not examined any effects away from half-filling or at incommensurate wave vectors here. We leave those tasks to another publication.

ACKNOWLEDGMENTS

This research was supported by the Office of Naval Research under Grant No. N00014-99-1-0328. We acknowledge useful discussions with T. Devereaux, D. Hess, J. Serene, and A. Shvaika.

APPENDIX: EQUIVALENCE TO THE ATOMIC DIAGRAMMATIC APPROACH

To compare our result with the diagrammatic approach,[5] we must begin with Shvaika's result for the frequency-dependent piece of the reducible vertex function,

$$\tilde{\Gamma}(i\omega_n,i\omega_{n'};i\nu_l\neq 0)=\frac{1}{T}\frac{\delta_{nn'}}{G_nG_{n'}G_{n+l}G_{n'+l}}\frac{U^2w_1(1-w_1)}{(i\omega_n+\mu-\lambda_n)(i\omega_n+\mu-\lambda_n-U)(i\omega_{n+l}+\mu-\lambda_{n+l})(i\omega_{n+l}+\mu-\lambda_{n+l}-U)}. \tag{A1}$$

By making the replacement $i\omega_n+\mu-\lambda_n=[G_0(i\omega_n)]^{-1}=(G_n)^{-1}+\Sigma_n$, the right-hand-side of Eq. (A1) is equivalent to

$$\frac{1}{T}\frac{\delta_{nn'}w_0w_1U^2}{(1+G_n\Sigma_n)[1+G_n(\Sigma_n-U)](1+G_{n+l}\Sigma_{n+l})[1+G_{n+l}(\Sigma_{n+l}-U)]}. \tag{A2}$$

Solving Dyson's equation for the irreducible vertex function, $\Gamma(i\omega_n,i\omega_{n'};i\nu_l\neq 0)$,

$$\tilde{\Gamma}(i\omega_n,i\omega_{n'};i\nu_l\neq 0)=\Gamma(i\omega_n,i\omega_{n'};i\nu_l\neq 0)-T\sum_{n''}\Gamma(i\omega_n,i\omega_{n''};i\nu_l\neq 0)G_{n''}G_{n''+l}\tilde{\Gamma}(i\omega_{n''},i\omega_{n'};i\nu_l\neq 0), \tag{A3}$$

then yields Eq. (46).

In order to prove that our simple result, Eq. (45), and the diagrammatic result, Eq. (46), are equivalent to each other, we first demonstrate the existence of a useful identity. Equation (40) can be expanded and multiplied by G_n to yield

$$w_1U=\Sigma_n(1-UG_n+\Sigma_nG_n), \tag{A4}$$

$$=\Sigma_{n+l}(1-UG_{n+l}+\Sigma_{n+l}G_{n+l}), \tag{A5}$$

where the second equation is evaluated equivalently, with $n\mapsto n+l$. Equation (A4) is used twice to simplify the product given below:

$$(1+G_n\Sigma_n)[1+G_n(\Sigma_n-U)]=1+G_n\Sigma_n-UG_n+w_1U \tag{A6}$$

$$=w_1U\left(\frac{1}{\Sigma_n}+G_n\right), \tag{A7}$$

and similarly for $n\mapsto n+l$.

Hence the expression on the right of Eq. (46) is rewritten as

$$\frac{1}{T}\frac{w_0w_1U^2}{w_1^2U^2(1/\Sigma_n+G_n)(1/\Sigma_{n+l}+G_{n+l})+G_nG_{n+l}w_0w_1U^2}, \tag{A8}$$

and multiplication of top and bottom by $(\Sigma_n-\Sigma_{n+l})\Sigma_n\Sigma_{n+l}$ leads to

$$\frac{1}{T}\frac{(\Sigma_n-\Sigma_{n+l})\Sigma_n\Sigma_{n+l}(1-w_1)}{w_1[\Sigma_n-\Sigma_{n+l}+G_n\Sigma_n(\Sigma_n-\Sigma_{n+l})+G_{n+l}\Sigma_{n+l}(\Sigma_n-\Sigma_{n+l})]+G_nG_{n+l}\Sigma_n\Sigma_{n+l}(\Sigma_n-\Sigma_{n+l})}. \tag{A9}$$

Now Eqs. (A4) and (A5) are further used to make the replacements $G_n\Sigma_n^2\mapsto w_1U-\Sigma_n+UG_n\Sigma_n$ and $G_{n+l}\Sigma_{n+l}^2\mapsto w_1U-\Sigma_{n+l}+UG_{n+l}\Sigma_{n+l}$ for all quadratic terms in the denominator. Numerous cancellations then lead to

$$\Gamma(i\omega_n,i\omega_n;i\nu_l\neq 0)=\frac{1}{T}\frac{(\Sigma_n-\Sigma_{n+l})\Sigma_n\Sigma_{n+l}(1-w_1)}{w_1(\Sigma_{n+l}\Sigma_nG_{n+l}-\Sigma_{n+l}\Sigma_nG_n)-\Sigma_{n+l}\Sigma_nG_{n+l}+\Sigma_{n+l}\Sigma_nG_n}, \tag{A10}$$

$$=\frac{1}{T}\frac{\Sigma_n-\Sigma_{n+l}}{G_n-G_{n+l}}, \tag{A11}$$

which yields our final result, Eq. (45).

[1] L. M. Falicov and J. C. Kimball, Phys. Rev. Lett. **22**, 997 (1969); R. Ramirez, L. M. Falicov, and J. C. Kimball, Phys. Rev. B **2**, 3383 (1970).

[2] U. Brandt and C. Mielsch, Z. Phys. B: Condens. Matter **75**, 365 (1989); **79**, 295 (1990).

[3] J. K. Freericks, Phys. Rev. B **47**, 9263 (1993); J. K. Freericks and R. Lemanski, *ibid.* **61**, 13 438 (2000).

[4] W. Metzner and D. Vollhardt, Phys. Rev. Lett. **62**, 324 (1989).

[5] A. M. Shvaika, Physica C (to be published), and private communication.

[6] J. K. Freericks and V. Zlatić, Phys. Rev. B **58**, 322 (1998).

[7] E. Müller-Hartmann, Z. Phys. B: Condens. Matter **74**, 507 (1989); **76**, 211 (1989).

[8] G. Baym and L. P. Kadanoff, Phys. Rev. **124**, 287 (1961).

[9] G. Baym, Phys. Rev. **127**, 1391 (1962).

[10] U. Brandt and M. P. Urbanek, Z. Phys. B: Condens. Matter **89**, 297 (1992).

[11] P. G. J. Van Dongen, Phys. Rev. B **45**, 2267 (1992).